Resonant two-photon ionization spectroscopy of jet-cooled Au_3

Gregory A. Bishea and Michael D. Morse
Department of Chemistry, University of Utah, Salt Lake City, Utah 84112.

(Received 5 June 1991; accepted 3 September 1991)

A band system of jet-cooled Au_3 has been located in the near infrared region of the spectrum using resonant two-photon ionization spectroscopy. The origin band is located at 13 354.15 cm^{-1} and the system extends more than 700 cm^{-1} further to the blue. The excited state displays a radiative lifetime of approximately 28 μs, corresponding to an absorption oscillator strength of $f \approx 0.0003$. Accordingly, it is thought that the transition corresponds to a spin-forbidden doublet ($S = 1/2$) to quartet ($S = 3/2$) transition, which is made allowed by spin–orbit contamination, presumably in the upper state. A progression in a totally symmetric stretching vibration ($\omega = 179.7$ cm^{-1}) is obvious in the spectrum, along with a much weaker progression in another mode, which displays an interesting pattern of splittings. Although no assignment is absolutely unambiguous, various candidates are presented. The most likely of these assigns the system as an $\tilde{A}\,^4E' \leftarrow \tilde{X}\,^2E'$ transition in the D_{3h} point group, with both the ground $\tilde{X}\,^2E'$ and excited $\tilde{A}\,^4E'$ states undergoing Jahn–Teller distortion. The vibronic levels of the $\tilde{A}\,^4E'$ state have been fitted assuming a linear Jahn–Teller effect in a system with *both* spin–orbit splitting and a significant anharmonicity in the Jahn–Teller active e' vibrational mode. The combined effects of anharmonicity in the Jahn–Teller active mode and spin–orbit coupling appear not to have been previously investigated; they are therefore examined in some detail.

I. INTRODUCTION

The homonuclear coinage and alkali metal clusters are systems of intense theoretical[1–19] and experimental[19–42] interest, in part because their chemical bonding in the ground electronic state is described rather simply by the interaction of a single s electron on each atom. The homonuclear trimers of these species are especially interesting for another reason as well. In D_{3h} symmetry, the s orbitals of the constituent atoms may be combined to give a three-center bonding molecular orbital of a_1' symmetry and a doubly degenerate, slightly antibonding molecular orbital of e' symmetry. With three valence s electrons, the ground electronic configuration is therefore $a_1'^2e'^1$, $^2E'$. According to the Jahn–Teller theorem, this state is orbitally degenerate and will therefore distort to a lower symmetry, removing the degeneracy in the process. For the homonuclear trimers, the distortion is from D_{3h} to C_{2v} symmetry, splitting the $^2E'$ state (in D_{3h}) into $^2A_1$ and $^2B_2$ states (in C_{2v}). This Jahn–Teller effect cannot occur in systems with fewer than three atoms, making the homonuclear alkali and coinage metal trimers the simplest examples of systems exhibiting this effect. As such, they are of great interest from both a theoretical and an experimental point of view.

In the preceding paper in this journal,[43] experimental results on the mixed coinage metal trimer species Cu_2Ag, Cu_2Au, and CuAgAu were presented. These systems are expected to possess conical intersections in their ground potential energy surfaces, but unlike their homonuclear cousins, the location of the conical intersections cannot be predicted by symmetry alone. The situation is quite different in the case of the homonuclear alkali and coinage metal trimers, where a conical intersection must occur at the D_{3h} geometry since the ground state is $^2E'$ under the D_{3h} symmetry group. In the present paper, we extend the studies reported for the Cu_2Ag, Cu_2Au, and CuAgAu molecules[43] to the homonuclear trimer Au_3. Electronic band systems have been observed previously for Cu_3[32–37] and Ag_3,[38] so the present study completes the initial spectroscopic survey of the homonuclear coinage metal trimers.

Theoretical calculations for Au_3 using the diatomics-in-molecules method have predicted an obtuse Jahn–Teller distortion from the D_{3h} ground state geometry, leading to a $^2B_2$ ground state.[11,12] *Ab initio* investigations employing relativistic effective core potentials in a complete active space self-consistent field (CASSCF) procedure followed by configuration interaction uniformly give an obtuse angled $^2B_2$ state lower in energy than the acute angled $^2A_1$ state, regardless of whether the $5d$ electrons are uncorrelated[13] or correlated in a complete active space self-consistent field/multireference single and double excitation configuration interaction (CASSCF/MRSDCI) procedure with 420 000 configurations.[14] The calculation in which the $5d$ electrons are uncorrelated, however, gives a linear, $^2\Sigma_u^+$ ground state to be slightly more stable than the obtuse $^2B_2$ state, although both were found to be more stable than the acute $^2A_1$ state.[13] The $^2B_2$ state was also found to be stabilized over the $^2A_1$ state in a SCF-MCPF approach.[15]

Experimentally, the neutral gold trimer has been isolated in a perdeuterobenzene matrix and observed using electron-spin resonance (ESR) spectroscopy.[39] The spectrum has been interpreted as being due to unpaired spin populations of 0.42 in the $6s$ orbitals on each of two equivalent gold atoms and a population of 0.06 in the $6s$ orbital on the unique gold atom.[39] Presumably the remaining unpaired spin density in this molecule resides in $6p$ and $5d$ orbital contributions, but this would be detected through anistropic contribu-

tions to the hyperfine parameters and these are too small to be detected. This is consistent with a $^2B_2$ electronic structure, which would place the lone electron in an orbital of b_2 symmetry, with large (and opposite) amplitudes on two equivalent atoms and a node on the third, unique gold atom.[39] Such an orbital would contribute to antibonding interactions between the two equivalent gold atoms and nonbonding interactions between each of these and the unique atom, leading to an opening up of the bond angle, giving an obtuse Jahn–Teller distortion.[39] This is consistent with all of the theoretical studies described above.

Other experimental information on Au_3 is given by a high temperature mass spectrometric study of the $Au + Au_2 \leftrightarrows Au_3$ equilibrium, which provides a third law estimate of the binding energy of $D_0^0(Au_2\text{–}Au) = 1.51 \pm 0.15$ eV and an estimate of the atomization energy of Au_3 as 3.80 ± 0.13 eV.[40] The binding energy of $D_0^0(Au_2\text{–}Au) = 1.51 \pm 0.15$ eV is less than the bond strength of Au_2 given by $D_0^0(Au_2) = 2.290 \pm 0.008$ eV.[44] This is expected, since the third valence electron of Au_3 goes into a somewhat antibonding orbital, presumably of b_2 symmetry, thereby reducing the bond strength of Au_3 as compared to Au_2. Optical spectra of Au_3 isolated in argon matrices have been reported at 471 and 292 nm by Klotzbücher and Ozin,[29] and more recently optical spectra of size-selected gold clusters have been obtained by Harbich and coworkers by neutralizing a mass-selected beam of gold cluster ions and "soft landing" them in a rare gas matrix.[41,42] In the present study, we report a weak absorption system of gas phase Au_3 which has not been observed in any of these matrix isolation investigations.

Within the group I B elements, gold is particularly interesting because of the importance of relativistic effects. In very simple terms, the large nuclear charge on gold allows the electrons which penetrate close to the nucleus to reach speeds approaching the speed of light. As a result, the mass of these penetrating electrons undergoes a relativistic increase according to $m = m_0(1 - v^2/c^2)^{-1/2}$. Since the atomic scale of length is defined by the Bohr radius $a_0 = \hbar^2/m_e e^2$, a relativistic *increase* in the mass of the electron, m_e, will lead to a corresponding relativistic *decrease* in the atomic scale of length. As a result, orbitals which penetrate close to the nucleus (including all s orbitals) undergo a relativistic contraction. On the other hand, nonpenetrating orbitals (such as d and f orbitals) are better shielded by the more contracted s orbitals and undergo a concomitant relativistic expansion, making them more accessible for chemical interactions. This relativistic effect makes the $6s$ orbital of gold smaller and less diffuse than the corresponding $5s$ orbital of silver, and for this reason Au_2 possesses a shorter bond length (2.4719 Å)[45] and greater bond strength (2.290 ± 0.008 eV)[44] than does Ag_2 (2.5310 Å,[46] 1.65 ± 0.03 eV[36]).

A brief experimental overview is presented in Sec. II. The spectrum of Au_3 is reported in Sec. III, followed by a discussion of possible assignments in Sec. IV. A summary of our most important results then concludes the paper in Sec. V. Details of the effects of anharmonicity in an $E \otimes e$ system undergoing a linear Jahn–Teller effect are given in Appendix A. This is extended to include the possibility of significant spin–orbit coupling in Appendix B.

II. EXPERIMENTAL

The experimental method used in the present investigation combines resonant two-photon ionization spectroscopy (R2PI) with time-of-flight mass spectrometric detection (TOFMS). The apparatus has been described in detail in a previous publication on the spectroscopy of Al_3.[47]

The source chamber couples a pulsed laser vaporization of a metallic sample with a subsequent supersonic expansion using helium carrier gas. A 99.95% pure gold foil ($25 \times 25 \times 0.5$ mm, Alfa Products) was used as the metal target in the present investigation. This was rotated continuously and translated using a rotating disk mount similar to that described by O'Brien *et al.*[48] The sample was vaporized using the second harmonic radiation from a Q-switched Nd:YAG laser (532 nm, $\approx$15 mJ/pulse), focused to a spot approximately 0.5 mm in diameter. Atoms ejected from the surface of the target disk were carried down a small channel 2 mm in diameter and 2 cm in length by a pulse of helium carrier gas, which was timed to coincide with the firing of the vaporization laser. Following this region, the metal clusters and carrier gas entered an extension channel 6 mm in length, tapering from a 5 mm initial inside diameter down to a 1.5 mm exit orifice. This extension channel was found to increase the production of triatomic gold prior to expansion into vacuum and the small exit orifice promoted excellent supersonic cooling. As a result, low rotational temperatures and narrow vibronic bands were obtained. Approximately 8 in. downstream, the beam was collimated by a 5 mm skimmer, which also served to separate the relatively high pressure source chamber (2×10^{-3} Torr) from the lower pressure interrogation chamber (1×10^{-5} Torr).

The interrogation region consisted of a Wiley–McLaren two-stage extraction assembly,[49] a reflecting electrostatic field, and a dual microchannel plate detector. The molecular beam was first probed with a tunable dye laser, pumped by either the second or third harmonic output from a Q-switched Nd:YAG laser. This process allowed an investigation of excited electronic states in the spectral range from approximately 370 to 900 nm. Ionization was accomplished with a fixed frequency excimer laser (ArF, 193 nm, 6.42 eV), which was chosen to have sufficient energy to photoionize excited states of Au_3, but which could not photoionize the ground state of Au_3 in a one-photon process. Ions generated by the resonant two-photon process were then extracted in the Wiley–McLaren source and accelerated into a time-of-flight (TOF) tube. A reflectron assembly was used to improve the mass resolution, although this was unnecessary in the present case because gold has only one naturally occurring isotope ^{197}Au. A dual microchannel plate detector at the base of the second TOF tube then detected the ions. The resulting signal was amplified, digitized, and signal averaged as the dye laser wavelength was scanned, thereby allowing the spectrum to be recorded.

Excited state lifetime measurements were performed by time-delayed resonant two-photon ionization techniques.

By varying the interval between the excitation and ionization laser pulses, the exponential decay of the excited state population was probed. The resulting ion signal as a function of delay interval was fitted to extract the excited state lifetime using a standard nonlinear least-squares algorithm.[50]

III. RESULTS

Figure 1 displays the low resolution R2PI vibronic spectrum of Au_3, obtained using LDS 750 and 751 dye laser radiation in conjunction with ArF radiation as the photoionization laser. Although the entire visible, near infrared, and near ultraviolet regions of the spectrum were scanned, only one band system was observed. Accordingly, it is labeled as the $\tilde{A} \leftarrow \tilde{X}$ system.

The observation of the $\tilde{A} \leftarrow \tilde{X}$ band system using ArF radiation to provide the second, photoionizing photon places the ionization potential (I.P.) of Au_3 in the range $6.42 < \text{I.P.}(Au_3) < 8.08$ eV. Although this covers a broad range, it is in agreement with the scaled vertical I.P. obtained by Partridge *et al.* of 7.06 eV.[19] In the scaling procedure employed by these authors, the correlation error which results from treating N electrons in the neutral and $N-1$ electrons in the ion is corrected empirically by scaling the calculated I.P. of Au_3 by the ratio of the known I.P. of atomic gold (Au) to the calculated value. This scaling method gives results for the ionization potentials of Cu_2, CuAg, CuAu, and Au_2 of 7.90, 7.62, 8.81, and 9.41 eV,[19] which are in excellent agreement with the experimental values of 7.899 ± 0.007,[51] 7.7806 ± 0.0004,[52] 8.74 ± 0.05,[53] and 9.20 ± 0.21 eV,[44] respectively. Assuming similar errors in the application of the scaling method to triatomic molecules, the I.P. of Au_3 probably falls in the range of 7.06 ± 0.3 eV.

Table I lists the observed vibronic bands and the measured excited state lifetimes determined for two of the upper state vibronic levels, which are 28.3 ± 2.1 and $27.1 \pm 1.1\,\mu$s. Assuming that the decay is dominated by fluorescence to the ground state, this excited state lifetime implies an absorption oscillator strength of $f \approx 0.0003$, making the $\tilde{A} \leftarrow \tilde{X}$ band system very weak indeed, similar in oscillator strength to that found for the $a\,^3\Sigma_u^+ \leftarrow X\,^1\Sigma_g^+$ transition of gold dimer.[44] Undoubtedly, this explains the failure of all matrix isolation studies[29,41,42] to observe this system in absorption. It also strongly suggests that the $\tilde{A}$ excited state is primarily quartet ($S = 3/2$) in character, making the $\tilde{A} \leftarrow \tilde{X}\,^2E'$ transition nominally spin forbidden.

The system shows a strong origin band at 13 354.15 cm^{-1} with an obvious progression of strong, sharp bands of gradually diminishing intensity proceeding toward the blue. Between these strong features, a number of weaker features are found which show an interesting pattern of splittings, discussed in greater detail below. The origin band is labeled $\tilde{A}_1 00^0$ and the strong, sharp members of the progression are labeled as $\tilde{A}_1 10^0$, $\tilde{A}_1 20^0$, $\tilde{A}_1 30^0$, and $\tilde{A}_1 40^0$. Anticipating the assignment of the system as an $\tilde{A}\,E' \leftarrow \tilde{X}\,^2E'$ system with spin–orbit splitting in the $\tilde{A}$ state, this labeling scheme identifies the quantum numbers of the $\tilde{A}$ state as follows: The prefix $\tilde{A}_1$ identifies the upper level of the transition as the

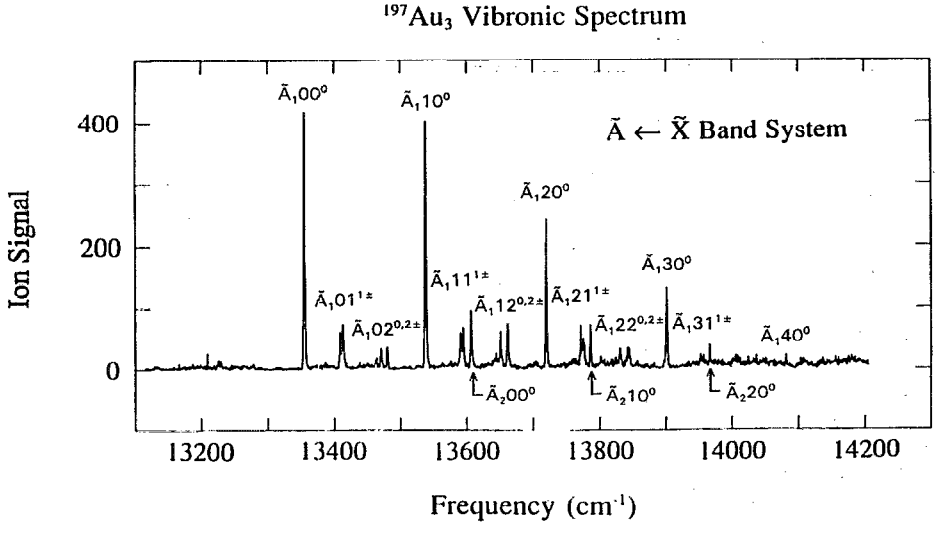

FIG. 1. Low resolution scan of the $\tilde{A} \leftarrow \tilde{X}$ band system of Au_3, recorded using LDS 750 and 751 dye laser radiation in combination with ArF excimer radiation for photoionization. The spectrum is tentatively assigned as an $\tilde{A}\,^4E' \leftarrow \tilde{X}\,^2E'$ transition in which the upper $\tilde{A}$ state undergoes significant spin–orbit splitting. Bands labeled by $\tilde{A}_1$ are assigned to the lower spin–orbit component, while the $\tilde{A}_2$ bands are assigned to a higher spin–orbit component. The bending mode is excited with one quantum in the pair of bands near 13 400 cm^{-1} and these bands (which would be degenerate in the absence of a Jahn–Teller effect) are split. Near 13 460 cm^{-1} are bands which correspond to excitation of the bending mode with two vibrational quanta, which are now split into a triplet of features by a combination of a Jahn–Teller effect and vibrational anharmonicity. All of the observed bands have been assigned and fitted to a model in which the upper state of the system undergoes a linear Jahn–Teller effect in combination with significant spin–orbit coupling and vibrational anharmonicity in the Jahn–Teller active bending mode.

TABLE I. Vibronic bands of the $\tilde{A}\leftarrow\tilde{X}$ system of Au_3.[a]

	$C_{2v}\leftarrow C_{2v}$ assignments[b]				
	Fit 1		Fit 2		
Observed frequency	Assignment[c]	Fit[d]	Assignment[c]	Fit[d]	Lifetime (μs)
13 354.15	0_0^0	13 354.20(− 5)	0_0^0	13 354.20(− 5)	28.3 ± 2.1
13 409.27	2_0^1	13 409.40(− 13)	3_0^2	13 409.40(− 13)	
13 413.00	3_0^2	13 412.68(32)	2_0^1	13 412.68(32)	
13 460.86	2_0^2	13 461.23(− 37)	3_0^4	13 461.23(− 37)	
13 469.38	$2_0^1 3_0^2$	13 468.94(44)	$2_0^1 3_0^2$	13 468.94(44)	
13 479.88	3_0^4	13 480.44(− 56)	2_0^2	13 480.44(− 56)	
13 535.87	1_0^1	13 535.87(0)	1_0^1	13 535.87(0)	
13 590.16	$1_0^1 2_0^1$	13 590.12(4)	$1_0^1 3_0^2$	13 590.12(4)	
13 593.78	$1_0^1 3_0^2$	13 593.56(22)	$1_0^1 2_0^1$	13 593.56(22)	
13 604.94	X		X		
13 641.26	$1_0^1 2_0^2$	13 640.98(28)	$1_0^1 3_0^4$	13 640.98(28)	
13 648.86	$1_0^1 2_0^1 3_0^2$	13 648.87(− 1)	$1_0^1 2_0^1 3_0^2$	13 648.87(− 1)	
13 660.64	$1_0^1 3_0^4$	13 660.54(10)	$1_0^1 2_0^2$	13 660.54(10)	
13 716.88	1_0^2	13 716.94(− 6)	1_0^2	13 716.94(− 6)	27.1 ± 1.1
13 770.59	$1_0^2 2_0^1$	13 770.24(35)	$1_0^2 3_0^2$	13 770.24(35)	
13 773.62	$1_0^2 3_0^2$	13 773.86(− 24)	$1_0^2 2_0^1$	13 773.86(− 24)	
13 784.05	$X 1_0^1$		$X 1_0^1$		
13 820.24	$1_0^2 2_0^2$	13 820.15(9)	$1_0^2 3_0^4$	13 820.15(9)	
13 827.78	$1_0^2 2_0^1 3_0^2$	13 828.21(− 43)	$1_0^2 2_0^1 3_0^2$	13 828.21(− 43)	
13 840.50	$1_0^2 3_0^4$	13 840.05(45)	$1_0^2 2_0^2$	13 840.05(45)	
13 897.14	1_0^3	13 897.43(− 29)	1_0^3	13 897.43(− 29)	
13 949.50	$1_0^3 2_0^1$	13 949.77(− 27)	$1_0^3 3_0^2$	13 949.77(− 27)	
13 953.26	$1_0^3 3_0^2$	13 953.56(− 30)	$1_0^3 2_0^1$	13 953.56(− 30)	
13 963.60	$X 1_0^2$		$X 1_0^2$		
14 077.72	1_0^4	14 077.32(40)	1_0^4	14 077.32(40)	

[a] All observed and fitted frequencies are given in wave numbers (cm^{-1}).

[b] $C_{2v}\leftarrow C_{2v}$ fits employ the expression

$$\nu = T_0 + \sum_i \left[\omega_i' v_i' + x_{ii}'(v_i'^2 + v_i)\right] + \sum_{i<j} x_{ij}'\left[v_i' v_j' + (v_i' + v_j')/2\right],$$

resulting in the following fitted constants (with 1σ error limits given in parentheses:

Parameter	Fit 1	Fit 2
T_0	13 354.20(33)	13 354.20(33)
ω_1'	182.94(50)	182.89(50)
ω_2'	58.80(92)	49.33(92)
ω_3'	25.69(44)	28.84(44)
x_{11}'	− 0.30(8)	− 0.30(8)
x_{22}'	− 1.69(25)	4.64(25)
x_{33}'	1.16(6)	− 0.42(6)
x_{12}'	− 0.96(15)	− 0.78(15)
x_{13}'	− 0.39(8)	− 0.48(8)
x_{23}'	0.53(21)	0.53(21)
χ^2	1.878	1.878

[c] Bands labeled as X, $X 1_0^1$, and $X 1_0^2$ are unexplained in these assignments.

[d] Residuals ($\nu_{obs} - \nu_{calc}$) are given in units of 0.01 cm^{-1} in parentheses after each fitted value.

lower of the two observed spin–orbit components of the $\tilde{A}$ state ($\tilde{A}_2$ is reserved for the upper spin–orbit component); the first numeral indicates the number of vibrational quanta of the totally symmetric breathing mode excited in the upper state; the second numeral indicates the number of vibrational quanta of the doubly degenerate bending mode which are excited in the upper electronic state. The superscripts designate the vibrational angular momentum quantum number l to which the upper state correlates as the Jahn–Teller splitting drops to zero, and the $\pm$ sign designates whether the upper level of the transition corresponds to the higher (+) or the lower (−) of the levels split by the Jahn–Teller ef-

fect. Since all of the observed transitions originate from the ground vibronic level of the ground electronic state, the quantum numbers of the lower state are suppressed for simplicity. Tables I and II list all of the observed transitions along with some possible assignments, as discussed in Sec. IV below.

The progression of strong, sharp bands is undoubtedly a progression in a totally symmetric mode of the molecule. Given that the origin band is as intense as the first member of this progression, that the intensity of this main progression falls off rather quickly with higher vibrational quanta, and that the remaining bands are all very weak, the change in equilibrium molecular geometry which accompanies the electronic excitation cannot be very severe. With this in mind, it makes sense to consider the possibilities of a linear ($D_{\infty h}$) to linear ($D_{\infty h}$) transition, a bent (C_{2v}) to bent (C_{2v}) transition, and an equilateral (D_{3h}) to equilateral (D_{3h}) transition. These possibilities are explored further in Sec. IV below.

In addition to the progression in a totally symmetric vibrational mode, the spectrum shows a doublet of bands near 13 411 cm^{-1} labeled $\tilde{A}_1 01^{1\pm}$ (about 57 cm^{-1} above the $\tilde{A}_1 00^0$ band) and a triplet of bands near 13 470 cm^{-1} labeled $\tilde{A}_1 02^{0,2\pm}$ (about 116 cm^{-1} above the $\tilde{A}_1 00^0$ band).

TABLE II. Vibronic bands of the $\tilde{A}\leftarrow\tilde{X}$ system of Au_3.[a]

	$D_{3h}\leftarrow D_{3h}$ assignment[b] $\tilde{A}\,E'\leftarrow\tilde{X}\,^2E'$				
Observed frequency	Assignment	Fit 1[c]	Assignment	Fit 2[d]	Lifetime (μs)
13 354.15	00^0	13 355.83(− 168)	$\tilde{A}_1 00^0$	13 355.97(− 182)	28.3 ± 2.1
13 409.27	01^{1-}	13 409.45(− 18)	$\tilde{A}_1 01^{1-}$	13 409.28(− 1)	
13 413.00	01^{1+}	13 413.30(− 30)	$\tilde{A}_1 01^{1+}$	13 413.56(− 56)	
13 460.86	02^{2-}	13 460.77(9)	$\tilde{A}_1 02^{2-}$	13 461.11(− 25)	
13 469.38	02^{2+}	13 468.44(94)	$\tilde{A}_1 02^{2+}$	13 468.32(106)	
13 479.88	02^0	13 480.22(− 34)	$\tilde{A}_1 02^0$	13 480.30(− 42)	
13 535.87	10^0	13 535.88(− 1)	$\tilde{A}_1 10^0$	13 535.93(− 6)	
13 590.16	11^{1-}	13 589.50(66)	$\tilde{A}_1 11^{1-}$	13 589.24(92)	
13 593.78	11^{1+}	13 593.35(43)	$\tilde{A}_1 11^{1+}$	13 593.53(26)	
13 604.94			$\tilde{A}_2 00^0$	13 604.15(79)	
13 641.26	12^{2-}	13 640.82(44)	$\tilde{A}_1 12^{2-}$	13 641.07(19)	
13 648.86	12^{2+}	13 648.49(37)	$\tilde{A}_1 12^{2+}$	13 648.29(58)	
13 660.64	12^0	13 660.27(37)	$\tilde{A}_1 12^0$	13 660.26(38)	
13 716.88	20^0	13 716.14(74)	$\tilde{A}_1 20^0$	13 716.14(74)	27.1 ± 1.1
13 770.59	21^{1-}	13 769.76(83)	$\tilde{A}_1 21^{1-}$	13 769.45(114)	
13 773.62	21^{1+}	13 773.61(1)	$\tilde{A}_1 21^{1+}$	13 773.73(− 11)	
13 784.05			$\tilde{A}_2 10^0$	13 784.12(− 7)	
13 820.24	22^{2-}	13 821.08(− 84)	$\tilde{A}_1 22^{2-}$	13 821.28(− 104)	
13 827.78	22^{2+}	13 828.75(− 97)	$\tilde{A}_1 22^{2+}$	13 828.49(− 71)	
13 840.50	22^0	13 840.53(− 3)	$\tilde{A}_1 22^0$	13 840.46(4)	
13 897.14	30^0	13 896.60(54)	$\tilde{A}_1 30^0$	13 896.59(55)	
13 949.50	31^{1-}	13 950.22(− 72)	$\tilde{A}_1 31^{1-}$	13 949.90(− 40)	
13 953.26	31^{1+}	13 954.07(− 81)	$\tilde{A}_1 31^{1+}$	13 954.18(− 92)	
13 963.60			$\tilde{A}_2 20^0$	13 964.32(− 72)	
14 077.72	40^0	14 077.27(45)	$\tilde{A}_1 40^0$	14 077.28(44)	

[a] All observed and fitted frequencies are given in wave numbers (cm^{-1}).

[b] In the $D_{3h}\leftarrow D_{3h}$ $^2E'\leftarrow{}^2E'$ assignment, only the upper level of the transition is designated. Since all transitions originate from the ground vibronic level of the ground electronic state, this introduces no ambiguity. The numerals indicate the number of quanta excited in the totally symmetric breathing mode and the number of quanta excited in the bending mode, respectively. Superscripts denote the vibrational angular momentum quantum number l and the ± superscript denotes whether the state is the higher (+) or lower (−) of the Jahn–Teller components associated with the state. For fit 2, the prefix $\tilde{A}_1$ indicates the lower spin–orbit component of the $\tilde{A}$ state, while $\tilde{A}_2$ indicates the higher spin–orbit component.

[c] Fit 1 employs the treatment of the linear Jahn–Teller effect with anharmonicity as described in Appendix A. Direct matrix diagonalization of Eq. (A7) was combined with a nonlinear least-squares fitting process, resulting in the following fitted constants: $T_0 = 13\,214.22$; $\omega_1 = 179.85$; $x_{11} = 0.102$; $\omega_2 = 51.04$; $x_{22} = 2.75$; $g = -3.89$; $k = 0.195$ (or $D = k^2/2 = 0.0191$) giving $\chi^2 = 9.584$.

[d] Fit 2 employs the treatment of the linear Jahn–Teller effect with spin–orbit coupling and anharmonicity as described in Appendix B. Direct matrix diagonalization of Eq. (B8) was combined with a nonlinear least-squares fitting process, resulting in the following fitted constants: $T_0 = 13\,323.86$; $\omega_1 = 179.72$; $x_{11} = 0.122$; $\omega_2 = 61.89$; $x_{22} = 2.32$; $g = -3.86$; $k = 0.7574$ (or $D = k^2/2 = 0.2869$); $\zeta = 228.60$ giving $\chi^2 = 12.509$.

Moreover, analogous doublets and triplets of bands are found built off the $\tilde{A}_1 1^0$ and $\tilde{A}_1 2^0$ bands, and a keen eye can discern a trace of the doublet built off the $\tilde{A}_1 3^0$ band. These additional features are spaced correctly to correspond to a single and a double excitation, respectively, in another normal mode. The splitting pattern is unusual, however, and may be used to make a preliminary assignment of the geometry and electronic character of the ground and excited states. In addition to these doublets and triplets, weak single features are found near 13 605, 13 784, and 13 964 cm^{-1}. As will be discussed below, these single features are the most perplexing features of the spectrum and their successful interpretation has required that the combined effects of spin–orbit coupling, anharmonicity in the e' bending mode, and a linear Jahn–Teller effect be considered.

IV. POSSIBLE ASSIGNMENTS OF THE $\tilde{A} \leftarrow \tilde{X}$ TRANSITION IN Au_3

A. Consideration of a linear ($D_{\infty h}$)←linear ($D_{\infty h}$) transition

Although most *ab initio* calculations are in agreement that the ground state of Au_3 derives from a Jahn–Teller distortion of an equilateral D_{3h} $^2E'$ state,[11,12,14,15] lower levels of theory predict a linear $^2\Sigma_u^+$ ground state.[13] Is the observed spectrum consistent with this possibility? If the ground state were a linear $^2\Sigma_u^+$ state, the totally symmetric, progression-forming mode would be the symmetric stretching vibration, and the much weaker doublet and triplet bands would have to correspond to excitations of the doubly degenerate bending mode. However, a single excitation of the doubly degenerate bending mode ($v_2 = 1$) of a linear molecule in a Σ state leads to a doubly degenerate vibronic level ($l = \pm 1$) of Π symmetry. No splitting of this doubly degenerate level is possible, except for l-type doublings, which are rotationally induced and would be unobservable at this level of resolution in a jet-cooled molecule where only the lowest rotational levels are populated. On this basis, an $\tilde{A}\ \Sigma_g \leftarrow \tilde{X}\ ^2\Sigma_u^+$ assignment of the transition may be removed from consideration.

If the upper state were an orbitally degenerate state, such as a Π_g state, the situation would be somewhat more complicated. In such cases, the Renner–Teller effect leads to splittings of the $v_2 = 1$ level, due to vibronic coupling of the vibrational angular momentum ($l = 1$) with the orbital electronic angular momentum ($\Lambda = 1$ for a Π_g state).[54–57] This leads to two vibronic levels of Σ_u symmetry and one vibronic level of Δ_u symmetry. However, if the transition is electronically $\Pi_g \leftarrow \Sigma_u$ in nature, the only upper state vibronic levels which may be observed in allowed transitions from the ground level are of Π_g symmetry. Thus, although the excited bending levels of a $^2\Pi_g$ state are split by vibronic interactions, one would not expect to observe any of the $v_2 = 1$ levels because of unfavorable selection rules.

From the measured excited state lifetime, it is likely that the upper state is primarily quartet ($S = 3/2$) in character, while a linear ground state would have to be $^2\Sigma_u^+$ in character. One might think that a combination of strong spin–orbit effects (which would be required to induce an $S = 3/2 \leftarrow S = 1/2$ transition) and the Renner–Teller effect might somehow make the $v_2 = 1$ levels observable. This cannot be the case, however, since the bending mode is of π_u symmetry and therefore the $v_2 = 1$ levels must always be opposite in g/u parity as compared to the $v_2 = 0$ level. It will therefore *never* be possible to observe both the $v_2 = 0$ and $v_2 = 1$ levels in optical transitions from the same lower state in any molecule of $D_{\infty h}$ symmetry. On this basis, we may rule out the possibility of a linear ($D_{\infty h}$) to linear ($D_{\infty h}$) transition for the $\tilde{A} \leftarrow \tilde{X}$ system of Au_3.

B. Consideration of a bent (C_{2v})←bent (C_{2v}) transition

If the upper and lower states of the molecule were well described as bent (C_{2v}) structures, then one would expect two vibrational modes to belong to the a_1 irreducible representation and the third would belong to the b_2 symmetry type. In an allowed electronic transition originating from the zero-point level of the ground state, the upper state must have a total vibrational symmetry of A_1. Accordingly, one would only expect to observe transitions of the type $1_0^i 2_0^j 3_0^{2k}$ occurring in the jet-cooled molecular beam. (The notation of $1_0^i 2_0^j 3_0^{2k}$ used here is the same as used in the preceding paper[43] and designates a transition in which mode 1 is excited from zero quanta in the ground state to i quanta in the excited state, while mode 2 is excited simultaneously from 0 to j quanta and mode 3 is excited simultaneously from 0 quanta in the ground state to $2k$ quanta in the excited state.) This situation can lead to apparent doublings and triplings of vibrational levels if the fundamental vibrational frequencies happen to exist in near whole number ratios, as was observed in the previous paper in the case of Cu_2Ag.[43] In the present case of the Au_3, the progression-forming mode (mode 1) would be the highest frequency mode and the frequency of mode 2 would have to be nearly equal to twice the frequency of mode 3 (the b_2 mode) to account for the observed pattern of vibrational levels. If this were the case, then the 2_0^1 and 3_0^2 transitions would be nearly degenerate, accounting for the bands near 13 411 cm^{-1}. Likewise, the 2_0^2, $2_0^1 3_0^2$, and 3_0^4 bands would be nearly degenerate, accounting for the triplet of features near 13 470 cm^{-1}. These doublets and triplets would be echoed at higher frequencies through their combinations with the 1_0^1, 1_0^2, and 1_0^3 bands. With suitable anharmonicities x_{ij}, the main progression and its attendant pattern of doublets and triplets of bands can be explained readily as a $C_{2v} \leftarrow C_{2v}$ transition. The results of two such fits are given in Table I.

Although both vibrational fits reproduce the observed band positions quite well, two problems remain with this assignment. First, is the requirement that the antisymmetric b_2 mode (mode 3) have a frequency of 25–28 cm^{-1}, which is necessary if one of the features near 13 411 cm^{-1} is to be assigned as the 3_0^2 band. Although metal molecules tend to have low vibrational frequencies, this value seems nearly out of the realm of reason. A second problem arises because the series of weak single features near 13 605, 13 784, and 13 964 cm^{-1} remain unexplained. Of course, it is conceivable that these features correspond to a second electronic state (or a

higher spin–orbit component of this state), but it seems unlikely that they could arise from a totally different excited state since their spacing is virtually identical to the spacing of the 1_0^i bands which make up the main progression. Finally, of course, *ab initio* theory predicts the ground state to be based on a Jahn–Teller distorted $^2E'$ state, so examination of this possibility offers the greatest hope for explaining the spectrum. Thus, although the $\tilde{A} \leftarrow \tilde{X}$ system can be partially accounted for as a $C_{2v} \leftarrow C_{2v}$ transition, a few problems remaining with this assignment make it an unlikely one.

C. Consideration of an equilateral (D_{3h}) ← equilateral (D_{3h}) transition

Finally, we must consider the Au_3 molecule as an equilateral triangle, which is the geometry most consistent with theoretical calculations. In D_{3h}, the vibrational modes of the molecule consist of a totally symmetric a_1' breathing mode and a doubly degenerate e' bending vibration. It is this latter vibration which can couple vibronically with an orbitally degenerate E' or E'' electronic state, leading to a Jahn–Teller distortion.[54,58–60] The best theoretical calculations are in agreement that the ground state is a $^2E'$ state in D_{3h} symmetry, which undergoes a mild Jahn–Teller distortion to remove the degeneracy.[14,15] These calculations are also in agreement that the $^2B_2$ component of the $^2E'$ state is a true minimum, while the $^2A_1$ component is a saddle point in the pseudorotation that converts the molecule from one of the three equivalent $^2B_2$ minima to another.[14,15] Since the electronic transition is undoubtedly induced by electric dipole radiation, one may consider upper states which may be reached by transitions polarized along the C_3 axis, or by transitions polarized perpendicular to this axis. The former case leads exclusively to $^2E''$ upper states, which will be Jahn–Teller active, while the latter case leads to $^2A_1'$, $^2A_2'$, and $^2E'$ upper states, of which only the $^2E'$ state is Jahn–Teller distorted.

1. Consideration of an $\tilde{A}\,^2E'' \leftarrow \tilde{X}\,^2E'$ transition

The lowest level of the $\tilde{X}\,^2E'$ ground state will always be an E' vibronic level and parallel transitions out of this level to an upper state of $^2E''$ symmetry can only go to E'' vibronic levels. Thus, all of the totally symmetric vibrational levels of the excited $^2E''$ state (which are of E'' total *vibronic* symmetry) can be reached by this process, thereby explaining the strong features in the $\tilde{A} \leftarrow \tilde{X}$ spectrum. However, the lowest excited bending level, corresponding to an excitation of the e' bending mode with one quantum of excitation, interacts with the $^2E''$ electronic state to produce A_1'', A_2'', and E'' vibronic levels (as given by the direct product of $E'' \otimes e'$).[58–60] Although a splitting of this first excited bending level into three levels is expected, only the E'' vibronic level may be accessed optically from the ground vibronic level of the ground electronic state. Therefore, if the transition were $^2E'' \leftarrow {}^2E'$ in symmetry, no doubling would be expected in the band near 13 411 cm^{-1}. On this basis, an $\tilde{A}\,^2E'' \leftarrow \tilde{X}\,^2E'$ transition may be excluded from consideration.

2. Consideration of $\tilde{A}\,^2A_1' \leftarrow \tilde{X}\,^2E'$ or $\tilde{A}\,^2A_2' \leftarrow \tilde{X}\,^2E'$ transitions

If the upper state were a nondegenerate $^2A_1'$ or $^2A_2'$ state, either of which could be accessed in a perpendicular transition from the ground $\tilde{X}\,^2E'$ state, the first excited bending level would remain doubly degenerate, having a vibronic symmetry of E'. Therefore, neither an $\tilde{A}\,^2A_1' \leftarrow \tilde{X}\,^2E'$ nor an $\tilde{A}\,^2A_2' \leftarrow \tilde{X}\,^2E'$ transition could give the observed doubling in the first excited level of the bending mode. These possibilities must therefore be removed from further consideration as well.

3. Consideration of an $\tilde{A}\,^2E' \leftarrow \tilde{X}\,^2E'$ transition

Finally, we consider the possibility of an $\tilde{A}\,^2E' \leftarrow \tilde{X}\,^2E'$ electronic transition, where once again both electronic states are subject to Jahn–Teller distortion.[58–60] In this case, the first excited bending level of the $\tilde{A}\,^2E'$ state would be split into components according to the direct product of the electronic and vibrational symmetries $E' \otimes e'$, which gives vibronic levels of A_1', A_2', and E' symmetry. All of these may be accessed in an (x,y)-polarized transition from the ground E' vibronic level of the ground $\tilde{X}\,^2E'$ state, since the transition dipole operator in this case would transform as E' and this interacts with an E' ground level to allow optical transitions to levels of A_1', A_2', and E' ($E' \otimes E'$) symmetry. One might therefore expect to observe a *triplet* of features in the 13 411 cm^{-1} band, in contrast to the doublet found in the spectrum of Fig. 1.

Examples of the Jahn–Teller effect can be further classified, however, into cases where only a linear effect is observed and those with a significant quadratic effect. The $E' \otimes e'$ vibronic problem,[58–66] which is appropriate to the $\tilde{A}\,^2E'$ and $\tilde{X}\,^2E'$ states of Au_3, is capable of showing both a linear and a quadratic Jahn–Teller effect. In the absence of quadratic effects, however, the A_1' and A_2' vibronic levels (which always occur in pairs) remain degenerate. Thus, the observed doubling of the band at 13 411 cm^{-1} is consistent with a linear Jahn–Teller effect, in which little or no quadratic effect is present. This would also imply little or no barrier to pseudorotation in the excited $\tilde{A}\,^2E'$ state, since a quadratic Jahn–Teller effect is required to introduce threefold minima into the adiabatic potential energy surface.[58–66]

A Jahn–Teller effect would also lead to a splitting of the vibrational levels in which two quanta of the bending mode are excited. This level would split into an a_1' level and a degenerate e' pair of levels even in the absence of a Jahn–Teller effect, simply due to anharmonic effects in the molecule. When combined with a $^2E'$ electronic state, however, a further splitting is expected. The vibronic levels deriving from this vibrational state may be obtained by taking the direct product of the electronic symmetry ($^2E'$) and the vibrational symmetry (a_1' or e') to obtain E' ($E' \otimes a_1'$) and E', A_1', and A_2' ($E' \otimes e'$) levels. Once again, if the Jahn–Teller effect is induced solely by linear coupling the A_1' and A_2' levels will remain degenerate, leading to a set of three distinct vibronic levels. This is in exact correspondence with the

observed spectrum, where the band near 13 470 cm^{-1} is split into a triplet of features.

The small splittings observed in the excited bending levels of the $\tilde{A}$ excited state of Au_3 would imply a small Jahn–Teller effect in which it might be expected that the second-order perturbation treatment first performed by Moffitt and Thorson[61] could account for the splittings. However, this theoretical treatment predicts equal splittings for the doublet of levels arising from one quantum of bending excitation and for the triplet of levels arising from two quanta of bending excitation. From Table I, it is clear that this is not the case in the $\tilde{A}$ state of Au_3, since the splitting within the doublets averages about 3.5 cm^{-1}, while the average spacings between components of the triplet are 7.9 and 11.7 cm^{-1}. According to Moffitt and Thorson,[61] Child,[62] and Herzberg,[54] the energies of the bending levels with v_2 bending quanta and a vibrational angular momentum l are given by

$$G(v_2,l) = \omega_2 (v_2 + 1) \mp 2D\omega_2 (l \pm 1), \qquad (4.1)$$

where only the upper signs are used for the case $l = 0$ and D is a coupling parameter defined in such a way that $D\omega_2$ is the difference in energy between the energy minimum of the potential energy surface in the D_{3h} geometry and the absolute energy minimum when a Jahn–Teller distortion to a C_{2v} geometry occurs. With this formula, it may be readily verified that the splittings expected in the $v_2 = 1$ and $v_2 = 2$ levels are $4D\omega_2$. Since the measured splittings vary between 3.5 and 11.7 cm^{-1}, this implies an energy stabilization of the distorted C_{2v} molecular geometry over the equilateral D_{3h} molecular geometry of about 1–3 cm^{-1}. Clearly this would be a very minor Jahn–Teller effect indeed, despite its rather dramatic effect on the appearance of the spectrum.

As mentioned above, however, the perturbation treatment predicts equal splittings, while our observed splittings vary by a factor of 3. Moreover, Child states that this treatment should be valid when $D < 0.5$.[62] Given an approximate value of ω_2 of 54 cm^{-1}, the observed splittings in the doublets would imply $D \approx 0.016$, which falls well within the range of applicability of Child's criterion. On the face of it, the variation in our measured splittings would appear to rule out an explanation of the vibronic structure of the $\tilde{A}$ state of Au_3 based on a Jahn–Teller effect. One important aspect has been neglected in the derivation of Moffitt and Thorson,[61] however. These authors have ignored the anharmonic aspects of the bending mode and it is precisely these anharmonic effects which lead to a splitting of the doubly excited bending level ($v_2 = 2$) into a_1' and e' vibrational levels in nondegenerate electronic states, such as a $^1A_1'$ state in the D_{3h} point group. If such splittings are of importance when Jahn–Teller effects are absent, it would be a mistake to expect them to vanish when the Jahn–Teller effect is present. In a quantitative treatment of the linear Jahn–Teller effect in an $E' \otimes e'$ vibronic problem, these anharmonic splittings would be expected to be most important when the Jahn–Teller stabilization is comparable in magnitude to the anharmonic splittings. This is precisely the situation in the present example.

Appendix A presents a derivation combining the effects of anharmonicity and a linear Jahn–Teller effect, demonstrating clearly that anharmonicity can cause the observed splittings to become nonuniform. With this derivation in hand, the secular equation (A7) has been used in a nonlinear least-squares fitting process[50] to fit the observed energy levels to the anharmonic linear Jahn–Teller model. The energies of the vibronic levels of the $\tilde{A}$ state obtained in this matrix diagonalization have been added to a constant T_0 to fit the observed transition frequencies. As is evident in Table II, the vibronic levels are very well reproduced with the fit and all parameters take on reasonable values.

The analysis of the $\tilde{A} \leftarrow \tilde{X}$ band system of Au_3 in terms of a linear Jahn–Teller effect with significant anharmonic effects is satisfying because it explains the spectrum in terms of weak effects which are expected in molecules of this type. However, there is one glaring flaw in this analysis—the series of single features near 13 605, 13 784, and 13 964 cm^{-1} remain unexplained. These fall in a region close to the expected positions of bands terminating on the $v_2 = 4$ levels, but there is no reason to expect that the splittings in the $v_2 = 4$ levels should vanish. Indeed, the Jahn–Teller fit of the other bands predicts that the $v_2 = 4$ levels are split into five levels differing in energy by 70 cm^{-1}. This is completely unlike the observed spectrum, where only a series of single features are obtained. It is also difficult to understand why a series of transitions terminating on $v_2 = 4$ should be observed so clearly while those terminating on $v_2 = 3$ are completely absent from the spectrum.

A possible explanation for these extra bands is that they correspond to an excited spin–orbit component of the $\tilde{A}$ state lying about 250 cm^{-1} above the lower spin–orbit level. Such a possibility is enticing, because it establishes a connection between these extra features and the fitted bands, and can therefore explain why the intervals between the extra bands are the same as those found in the main progression. If this assignment is to be considered, however, the previous fit (which omits the extra bands and ignores spin–orbit coupling) must be completely redone. It is well-known that the spin–orbit effect tends to quench the Jahn–Teller effect in systems with half-integral spin, so a much larger linear Jahn–Teller effect will be required to explain the spectrum if spin–orbit coupling is invoked.[54,67] At the same time, Ham[68] has shown that the Jahn–Teller effect can dramatically reduce the magnitude of the spin–orbit coupling, resulting in what is termed the Ham reduction or Ham effect.[58,60] Thus the two effects tend to suppress one another with the Jahn–Teller effect reducing the magnitude of the spin–orbit coupling and the spin–orbit splitting reducing the splittings resulting from a given linear Jahn–Teller parameter D.

Appendix B presents a derivation combining the effects of spin–orbit coupling, anharmonicity in the Jahn–Teller active mode, and a linear Jahn–Teller effect in the $E \otimes e$ vibronic problem. With this derivation in hand, the secular equation (B8) has been used in a nonlinear least-squares fitting process[50] to obtain a fit of the observed energy levels. The energies of the vibronic levels of the $\tilde{A}$ state obtained in this matrix diagonalization have been added to a constant T_0 to fit the observed transition frequencies. As is evident in Table II, the fit is quite good, reproducing all of the observed

bands to within 2 cm^{-1}. Moreover, the vibrational constants are reasonable, lending further credence to the assignment of the system as an $\tilde{A}\,E' \leftarrow \tilde{X}\,^2E'$ system, in which both the upper and lower states undergo a Jahn–Teller effect.

In this fit, the spin–orbit splitting of the $\tilde{X}\,^2E'$ ground state is assumed to be negligible. Despite the large magnitude expected for spin–orbit effects in a heavy element such as gold, this assumption is not unreasonable. First, the ground state of Au_3 undoubtedly derives from the interaction of three $5d^{10}6s^1$, $^2S_{1/2}$ ground state atoms. Thus, there is no electronic orbital angular momentum in the ground state (and as a result there can be no spin–orbit splitting), except to the extent that an admixture of higher-lying electronic configurations may contribute to this state. Second, the small residual spin–orbit splitting of the ground electronic state deriving from an admixture of higher electronic configurations will still be subject to the Ham reduction effect, resulting in a further diminishment of the spin–orbit splitting. The combination of both effects may well reduce the spin–orbit splitting of the ground state to a negligible value.

The observation of the series of weaker singlet features in the $\tilde{A}$ state and their assignment to an excited spin–orbit level of this state implies a much greater spin–orbit splitting in this state. This should come as little surprise, since the excited $\tilde{A}$ state undoubtedly possesses some character associated with the promotion of a $5d$ electron to a $6s$ orbital, at least on one of the atoms. Given a spin–orbit parameter of $\zeta_{Au}(5d) = 5097\ cm^{-1}$ for the free atom,[69] it is obvious from the fit that the Ham reduction effect leads to a serious diminishment of this value in the $\tilde{A}$ state of Au_3.

Finally, it should be noted that although Appendix B deals with the case of spin–orbit coupling in a Jahn–Teller active ^2E state, very similar effects are expected in E states of higher multiplicity. With the very long fluorescence decay times of the $\tilde{A}$ state in mind, the $\tilde{A}$ state may tentatively be assigned as a $^4E'$ state, with a spin–orbit splitting of approximately 229 cm^{-1}. A $^4E'$ state cannot arise from excitation of the σ framework, as in an $a_1'^1e'^2 \leftarrow a_1'^2e'^1$ excitation, since the $a_1'^1e'^2$ configuration can only give $^2A_1'$, $^2A_2'$, $^2E'$, and $^4A_2'$ molecular terms. Presumably the $\tilde{A}\,^4E'$ state then derives from excitation of a $5d$ electron on one of the gold atoms into the $6s$-based e' orbital, giving an electron configuration for the $\tilde{A}$ state of $5d^9_A 5d^{10}_B 5d^{10}_C a_1'^2e'^2$. The $\tilde{A}$ excited state then undoubtedly borrows oscillator strength for the $\tilde{A}\,^4E' \leftarrow \tilde{X}\,^2E'$ transition from a doublet ($S = 1/2$) state. The difference in absorption intensity for the upper and lower spin–orbit components of the $\tilde{A}$ state which is evident in Fig. 1 presumably reflects the details of the intensity borrowing mechanism, which may well be dependent on the spin–orbit level.

V. SUMMARY

A complicated vibronic band system, designated as the $\tilde{A} \leftarrow \tilde{X}$ system, has been observed in Au_3 using the resonant two-photon ionization technique. Based on the long (28 μs) lifetime of the upper state, it is assumed that the transition is primarily doublet ($S = 1/2$) to quartet ($S = 3/2$) in character. The spectrum is dominated by a progression in a single totally symmetric mode, which is presumably the a_1' breathing mode of an equilateral, D_{3h}-based structure. A short, weak progression in a second normal mode is also observed, with the first member split into a doublet and the second member split into a triplet of features. Finally, another series of single bands is also found, with the same spacing as the main progression, but lying some 250 cm^{-1} higher in energy.

Various possible assignments for the upper and lower states have been considered and it is concluded that the band system is best described as an $\tilde{A}\,^4E' \leftarrow \tilde{X}\,^2E'$ transition, where both the upper and lower states undergo a Jahn–Teller distortion. Since all of the observed transitions originate from the ground vibronic level of the ground electronic state, little can be ascertained about the ground state. On the other hand, 25 vibronic levels have been observed for the $\tilde{A}$ excited state and these have been fitted assuming that the excited $^4E'$ state undergoes a linear Jahn–Teller effect with spin–orbit splitting and significant anharmonicity in the Jahn–Teller active, doubly degenerate bending mode. This has required an examination of the combined effects of spin–orbit coupling and anharmonicity in the Jahn–Teller active mode, which appears not to have been previously investigated; accordingly these effects have been examined in some detail.

ACKNOWLEDGMENTS

Research support from the NSF under grant number CHE-8912673 is gratefully acknowledged. Acknowledgement is also made to the Donors of the Petroleum Research Fund, administered by the American Chemical Society, for partial support of this research.

APPENDIX A: THE LINEAR $E' \otimes e'$ JAHN–TELLER EFFECT WITH ANHARMONIC EFFECTS

Longuet-Higgins *et al.* have provided an excellent description of the $E \otimes e$ vibronic problem, with the clarity of exposition one would normally expect from a textbook.[62] These authors consider the motion of an electron on a deformable ring and show that the doubly degenerate electronic state characterized by an electronic orbital angular momentum of ± 1 can be considered in an electronic basis in which the electron moves with either positive (ψ_{elec}^{+}) or negative (ψ_{elec}^{-}) angular momentum. Since both electronic states become degenerate at the D_{3h} geometry, it is necessary to consider the total vibronic wave function to have contributions from both electronic states, giving a total vibronic wave function of the form

$$\Psi = \psi_{vib}^{+}(r,\phi)\psi_{elec}^{+} + \psi_{vib}^{-}(r,\phi)\psi_{elec}^{-}, \qquad \text{(A1)}$$

where r and ϕ represent the magnitude and phase of the displacement of the atoms in the doubly degenerate bending vibration. This differs from the standard Born–Oppenheimer or adiabatic treatment in that *two* potential energy surfaces are considered explicitly and are treated on an equal footing. In the absence of Jahn–Teller and anharmonic effects, the doubly degenerate bending vibration would be well described by the two-dimensional isotropic harmonic oscil-

lator wave functions of Pauling and Wilson[70] or of Townes and Schawlow,[71] which we denote here by $\chi_{n,m}(r,\phi)$, where

$$\chi_{n,m}(r,\phi) = N_{nm}\rho^{|m|}\exp(-\rho^2/2)F^{|m|}_{(1/2)(n+|m|)}(\rho^2)e^{im\phi}, \tag{A2}$$

where $n = 0,1,2,...$; $m = n, n-2,..., -n$; N_{nm} is a normalization constant; ρ is a reduced displacement coordinate which is proportional to r; and $F^{|m|}_{(1/2)(n+|m|)}$ is an associated Laguerre polynomial.[71] Here n gives the number of quanta of vibrational excitation in the doubly degenerate vibrational mode and m represents the vibrational angular momentum quantum number. Note that the vibrational quantum number n defined by Longuet-Higgins *et al.*[62] is equal to that used here plus one.

Longuet-Higgins *et al.* then demonstrate that the vibrational amplitudes that multiply each electronic amplitude obey a set of coupled differential equations given by

$$\begin{bmatrix} H_0 - E & kre^{-i\phi} \\ kre^{+i\phi} & H_0 - E \end{bmatrix}\begin{bmatrix} \psi^+_{vib}(r,\phi) \\ \psi^-_{vib}(r,\phi) \end{bmatrix} = 0. \tag{A3}$$

The off-diagonal terms involving $e^{\pm i\phi}$ lead to couplings between vibrational basis wave functions differing by one unit in m and this leads to the splitting of vibronic levels in the $E\otimes e$ vibronic problem. The vibrational amplitudes $\psi^+_{vib}(r,\phi)$ and $\psi^-_{vib}(r,\phi)$ may then be expanded in terms of the two-dimensional isotropic harmonic oscillator basis functions (A2) to obtain a final set of coupled equations

$$\begin{bmatrix} (m+1)\omega - E & k\omega\sqrt{(m+1)} & 0 & 0 & 0 & \cdots \\ k\omega\sqrt{(m+1)} & (m+2)\omega - E & k\omega\sqrt{1} & 0 & 0 & \cdots \\ 0 & k\omega\sqrt{1} & (m+3)\omega - E & k\omega\sqrt{(m+2)} & 0 & \cdots \\ 0 & 0 & k\omega\sqrt{(m+2)} & (m+4)\omega - E & k\omega\sqrt{2} & \cdots \\ 0 & 0 & 0 & k\omega\sqrt{2} & (m+5)\omega - E & \cdots \\ 0 & 0 & 0 & 0 & k\omega\sqrt{(m+3)} & \cdots \\ \cdots & \cdots & \cdots & \cdots & \cdots & \cdots \end{bmatrix}\begin{bmatrix} a_1 \\ a_2 \\ a_3 \\ a_4 \\ a_5 \\ a_6 \\ \vdots \end{bmatrix} = 0, \tag{A4}$$

where m can equal 0, 1, 2,..., ω is the frequency of the unperturbed doubly degenerate oscillator, and k is the coefficient of linear coupling in the Jahn–Teller effect, as given in Eq. (A3). In this expression, a_1, a_2, a_3, etc. represent the coefficients in the expansion of $\psi^+_{vib}(r,\phi)$ and $\psi^-_{vib}(r,\phi)$ in terms of the two-dimensional isotropic harmonic oscillator wave functions as

$$\psi^+_{vib}(r,\phi) = a_1\chi_{m,m}(r,\phi) + a_3\chi_{m+2,m}(r,\phi) + a_5\chi_{m+4,m}(r,\phi) + \cdots,$$
$$\psi^-_{vib}(r,\phi) = a_2\chi_{m+1,m+1}(r,\phi) + a_4\chi_{m+3,m+1}(r,\phi) + a_6\chi_{m+5,m+1}(r,\phi) + \cdots. \tag{A5}$$

The explicit matrix formulation given by Eq. (A4) is amenable to numerical calculations and may also be solved to second order in perturbation theory to obtain the energies given by Eq. (4.1), where k^2 has been replaced by $2D$, as is used by Child.[64]

It is the aim of this Appendix to generalize these results to a case in which the anharmonicity of the doubly degenerate bending mode exerts a comparable influence on the vibronic energy levels as does the linear Jahn–Teller effect. In such a case, one may replace the diagonal matrix elements in Eq. (A4) by the energy of the anharmonic doubly degenerate bending oscillator, which is given as

$$G(v_2,l) = \omega(v_2+1) + x(v_2+1)^2 + gl^2, \tag{A6}$$

where x and g provide the anharmonic corrections to the energies and the vibronic coupling is still taken to be given by the off-diagonal terms in Eq. (A4). With this modification, the secular equation associated with Eq. (A4) becomes

$$\begin{vmatrix} F(m) + m^2g - E & k\omega\sqrt{(m+1)} & 0 & 0 & \cdots \\ k\omega\sqrt{(m+1)} & F(m+1) + (m+1)^2g - E & k\omega\sqrt{1} & 0 & \cdots \\ 0 & k\omega\sqrt{1} & F(m+2) + m^2g - E & k\omega\sqrt{(m+2)} & \cdots \\ 0 & 0 & k\omega\sqrt{(m+2)} & F(m+3) + (m+1)^2g - E & \cdots \\ 0 & 0 & 0 & k\omega\sqrt{2} & \cdots \\ 0 & 0 & 0 & 0 & \cdots \\ \cdots & \cdots & \cdots & \cdots & \cdots \end{vmatrix} = 0, \tag{A7}$$

where $F(n)$ is given by

$$F(n) = (n+1)\omega + (n+1)^2x. \tag{A8}$$

Since each zeroth-order state is coupled to at most two other states in Eq. (A7), it is a simple matter to obtain estimates of the solutions E_p to Eq. (A7) by second-order perturbation theory. For a given value of m (0, 1, 2, etc.), the solutions to Eq. (A7) may be ordered according to energy by an index p, giving the following energies which are correct through second order in perturbation theory, where k^2 has again been replaced by $2D$:

TABLE III. Anharmonic $E \otimes e$ Jahn–Teller energy levels.[a]

m	p	v'	Energy
0	1	0^0	$\omega + x - 2D\omega + 6Dx + 2Dg$
0	2	1^{1+}	$2\omega + 4x + g + 4Dx - 4Dg$
1	1	1^{1-}	$2\omega + 4x + g - 4D\omega + 20Dx + 12Dg$
0	3	2^0	$3\omega + 9x - 2D\omega + 18Dx + 6Dg$
1	2	2^{2+}	$3\omega + 9x + 4g + 2D\omega - 6Dx - 18Dg$
2	1	2^{2-}	$3\omega + 9x + 4g - 6D\omega + 42Dx + 30Dg$
0	4	3^{1+}	$4\omega + 16x + g + 8Dx - 8Dg$
1	3	3^{1-}	$4\omega + 16x + g - 4D\omega + 40Dx + 24Dg$
2	2	3^{3+}	$4\omega + 16x + 9g + 4D\omega - 24Dx - 40Dg$
3	1	3^{3-}	$4\omega + 16x + 9g - 8D\omega + 72Dx + 56Dg$
0	5	4^0	$5\omega + 25x - 2D\omega + 30Dx + 10Dg$
1	4	4^{2+}	$5\omega + 25x + 4g + 2D\omega - 10Dx - 30Dg$
2	3	4^{2-}	$5\omega + 25x + 4g - 6D\omega + 70Dx + 50Dg$
3	2	4^{4+}	$5\omega + 25x + 16g + 6D\omega - 50Dx - 70Dg$
4	1	4^{4-}	$5\omega + 25x + 16g - 10D\omega + 110Dx + 90Dg$

[a] Calculated by second-order perturbation theory according to formulas (A10a) and (A10b). The $\pm$ signs associated with v' simply designate whether the level is raised (+) or lowered (−) as the Jahn–Teller coupling D is increased from zero.

For $p = 1, 3, 5, \ldots$,

$$E_p = (m+p)\omega + (m+p)^2 x + m^2 g + D\omega^2(p-1)/[\omega + (2m+2p-1)x - (2m+1)g] - D\omega^2(2m+p+1)/[\omega + (2m+2p+1)x + (2m+1)g] \quad \text{(A9a)}$$

and for $p = 2, 4, 6, \ldots$,

$$E_p = (m+p)\omega + (m+p)^2 x + (m+1)^2 g + D\omega^2(2m+p)/[\omega + (2m+2p-1)x + (2m+1)g] - (pD\omega^2)/[\omega + (2m+2p+1)x - (2m+1)g]. \quad \text{(A9b)}$$

These expressions simplify if $|x| \ll \omega/(2m+2p)$ and $|g| \ll \omega/(2m+1)$, giving for $p = 1, 3, 5, \ldots$,

$$E_p = (m+p)\omega + (m+p)^2 x + m^2 g - (2m+2)D\omega + Dx(m+p)(4m+6) + Dg(m+p)(4m+2) \quad \text{(A10a)}$$

and for $p = 2, 4, 6, \ldots$,

$$E_p = (m+p)\omega + (m+p)^2 x + (m+1)^2 g + 2mD\omega + Dx(m+p)(2-4m) - Dg(m+p)(2+4m). \quad \text{(A10b)}$$

Identifying the coefficient of g as l^2 and the coefficient of ω as $v+1$, the lowest vibronic levels v' are obtained as listed in Table III. This table demonstrates that when $D\omega$ and g are of similar magnitudes, the $v = 2$ triplet of levels will be asymmetrically split. This is in agreement with our observed spectrum.

APPENDIX B: THE LINEAR $E' \otimes e'$ JAHN–TELLER EFFECT WITH ANHARMONIC EFFECTS

In Appendix A, the effects of anharmonicity were combined with the linear Jahn–Teller effect to demonstrate that anharmonic effects can lead to nonuniform splittings in the vibronic levels of a ^1E molecule in D_{3h} symmetry. In this appendix, these results are further generalized to include the spin–orbit interaction as well. A nice discussion of the effects of spin–orbit coupling in the $E \otimes e$ vibronic problem has been given by Chau and Karlsson[67] and this provides the starting point for the present development.

In the linear Jahn–Teller effect in a ^1E state in the D_{3h} point group, it was necessary to consider two electronic states with positive and negative values of the component of electronic orbital angular momentum along the C_3 axis and these were designated by ψ_{elec}^{+} and ψ_{elec}^{-}, respectively. In a $^2E'$ molecule, these must be combined with the spin of the unpaired electron to give four distinct electronic states designated by $\psi_{\text{elec}}^{+}\alpha$, $\psi_{\text{elec}}^{-}\alpha$, $\psi_{\text{elec}}^{+}\beta$, and $\psi_{\text{elec}}^{-}\beta$, respectively. One might consider the most general formulation of the total (vibrational plus electronic) wave function to then consist of four terms, giving

$$\Psi = \psi_{\text{vib}}^{+\alpha}(r,\phi)\psi_{\text{elec}}^{+\alpha} + \psi_{\text{vib}}^{-\alpha}(r,\phi)\psi_{\text{elec}}^{-\alpha} + \psi_{\text{vib}}^{+\beta}(r,\phi)\psi_{\text{elec}}^{+\beta} + \psi_{\text{vib}}^{-\beta}(r,\phi)\psi_{\text{elec}}^{-\beta}, \quad \text{(B1)}$$

where r and ϕ represent the magnitude and phase of the displacement of the atoms in the doubly degenerate bending vibration, and explicit designation of the totally symmetric breathing mode is suppressed. Chau and Karlsson[67] demonstrate, however, that the vibronic coupling which induces the Jahn–Teller effect can only couple components with the same spin (α or β), so the secular equation for the vibrational amplitudes $\psi_{\text{vib}}^{+\alpha}(r,\phi)$, $\psi_{\text{vib}}^{-\alpha}(r,\phi)$, $\psi_{\text{vib}}^{+\beta}(r,\phi)$, and $\psi_{\text{vib}}^{-\beta}(r,\phi)$ reduces to the form

$$\begin{bmatrix} H_0 - \zeta/2 - E & kre^{-i\phi} & 0 & 0 \\ kre^{+i\phi} & H_0 + \zeta/2 - E & 0 & 0 \\ 0 & 0 & H_0 + \zeta/2 - E & kre^{-i\phi} \\ 0 & 0 & kre^{+i\phi} & H_0 - \zeta/2 - E \end{bmatrix} \begin{bmatrix} \psi_{\text{vib}}^{+\alpha}(r,\phi) \\ \psi_{\text{vib}}^{-\alpha}(r,\phi) \\ \psi_{\text{vib}}^{+\beta}(r,\phi) \\ \psi_{\text{vib}}^{-\beta}(r,\phi) \end{bmatrix} = 0, \quad \text{(B2)}$$

where the spin–orbit energy of the $\psi^{+}_{\text{elec}}\alpha$ and $\psi^{-}_{\text{elec}}\beta$ electronic states is given by $-\zeta/2$, while that of the $\psi^{-}_{\text{elec}}\alpha$ and $\psi^{+}_{\text{elec}}\beta$ states is given by $+\zeta/2$. An important new feature of this secular equation is that the linear Jahn–Teller portion of the Hamiltonian couples one spin–orbit component to the other, but causes no direct coupling within the vibrational levels of a particular spin–orbit component. As a result, large spin–orbit interactions ($\zeta \gg \omega$) cause the Jahn–Teller splittings to be reduced, since the energy difference between the coupled levels is governed by the magnitude of ζ.

This secular equation (B2) obviously block diagonalizes into portions involving the α and β spin states given by

$$\begin{bmatrix} H_0 - \zeta/2 - E & kre^{-i\phi} \\ kre^{+i\phi} & H_0 + \zeta/2 - E \end{bmatrix} \begin{bmatrix} \psi^{+\alpha}_{\text{vib}}(r,\phi) \\ \psi^{-\alpha}_{\text{vib}}(r,\phi) \end{bmatrix} = 0 \tag{B3}$$

and

$$\begin{bmatrix} H_0 + \zeta/2 - E & kre^{-i\phi} \\ kre^{+i\phi} & H_0 - \zeta/2 - E \end{bmatrix} \begin{bmatrix} \psi^{+\beta}_{\text{vib}}(r,\phi) \\ \psi^{-\beta}_{\text{vib}}(r,\phi) \end{bmatrix} = 0, \tag{B4}$$

respectively. These two equations may be combined to give

$$\begin{bmatrix} H_0 \mp \zeta/2 - E & kre^{-i\phi} \\ kre^{+i\phi} & H_0 \pm \zeta/2 - E \end{bmatrix} \begin{bmatrix} \psi^{+}_{\text{vib}}(r,\phi) \\ \psi^{-}_{\text{vib}}(r,\phi) \end{bmatrix} = 0, \tag{B5}$$

where it is understood that the upper/lower signs pertain to the α/β spin state. The vibrational amplitudes $\psi^{+}_{\text{vib}}(r,\phi)$ and $\psi^{-}_{\text{vib}}(r,\phi)$ may then be expanded in terms of the two-dimensional isotropic harmonic oscillator basis functions (A2) to obtain a final set of coupled equations

$$\begin{bmatrix} (m+1)\omega \mp \zeta/2 - E & k\omega\sqrt{(m+1)} & 0 & 0 & \cdots \\ k\omega\sqrt{(m+1)} & (m+2)\omega \pm \zeta/2 - E & k\omega\sqrt{1} & 0 & \cdots \\ 0 & k\omega\sqrt{1} & (m+3)\omega \mp \zeta/2 - E & k\omega\sqrt{(m+2)} & \cdots \\ 0 & 0 & k\omega\sqrt{(m+2)} & (m+4)\omega \pm \zeta/2 - E & \cdots \\ 0 & 0 & 0 & k\omega\sqrt{2} & \cdots \\ 0 & 0 & 0 & 0 & \cdots \\ \cdots & \cdots & \cdots & \cdots & \cdots \end{bmatrix} \begin{bmatrix} a_1 \\ a_2 \\ a_3 \\ a_4 \\ a_5 \\ a_6 \\ \vdots \end{bmatrix} = 0, \tag{B6}$$

where m can equal 0, 1, 2,..., ω is the frequency of the unperturbed doubly degenerate oscillator, and k is the coefficient of linear coupling in the Jahn–Teller effect, as given in Eqs. (A3) and (B2–B5). This equation is identical to that given by Eq. (A4) except that additional terms of $\pm\zeta/2$ are present in the diagonal matrix elements. In this expression, a_1, a_2, a_3, etc. represent the coefficients in the expansion of $\psi^{+}_{\text{vib}}(r,\phi)$ and $\psi^{-}_{\text{vib}}(r,\phi)$ in terms of the two-dimensional isotropic harmonic oscillator wave functions (A2) as

$$\psi^{+}_{\text{vib}}(r,\phi) = a_1\chi_{m,m}(r,\phi) + a_3\chi_{m+2,m}(r,\phi) + a_5\chi_{m+4,m}(r,\phi) + \cdots,$$
$$\psi^{-}_{\text{vib}}(r,\phi) = a_2\chi_{m+1,m+1}(r,\phi) + a_4\chi_{m+3,m+1}(r,\phi) + a_6\chi_{m+5,m+1}(r,\phi) + \cdots. \tag{B7}$$

The secular determinant of Eq. (B6) may be further generalized to include the effects of anharmonicity in the Jahn–Teller active bending mode, in exactly the same manner as was done in Appendix A, giving

$$\begin{vmatrix} F(m) + m^2g \mp \zeta/2 - E & k\omega\sqrt{(m+1)} & 0 & 0 & \cdots \\ k\omega\sqrt{(m+1)} & F(m+1) + (m+1)^2g \pm \zeta/2 - E & k\omega\sqrt{1} & 0 & \cdots \\ 0 & k\omega\sqrt{1} & F(m+2) + m^2g \mp \zeta/2 - E & k\omega\sqrt{(m+2)} & \cdots \\ 0 & 0 & k\omega\sqrt{(m+2)} & F(m+3) + (m+1)^2g \pm \zeta/2 - E & \cdots \\ 0 & 0 & 0 & k\omega\sqrt{2} & \cdots \\ 0 & 0 & 0 & 0 & \cdots \\ \cdots & \cdots & \cdots & \cdots & \cdots \end{vmatrix} = 0, \tag{B8}$$

where $F(n)$ is given by Eq. (A8).

This form is well suited for numerical computations, since the matrix is already in tridiagonal form. In addition, since each zeroth-order state is coupled to at most two other states, it is a simple matter to obtain estimates of the solutions to Eq. (B8) by second-order perturbation theory, precisely as was done in Appendix A. With the replacement of k^2 with $2D$, this gives

TABLE IV. Anharmonic $E \otimes e$ Jahn–Teller energy levels with spin–orbit coupling.[a]

Lower spin–orbit state			
m	p	v^l	Energy
0	1	0^0	$\omega + x - \zeta/2 - 2D\omega^2/(\omega+\zeta) + [6Dx\omega^2(\omega^2+\zeta^2) - 12Dx\omega^3\zeta + 2Dg\omega^2(\omega^2+\zeta^2) - 4Dg\omega^3\zeta]/(\omega^2-\zeta^2)^2$
1	1	1^{1-}	$2\omega + 4x + g - \zeta/2 - 4D\omega^2/(\omega+\zeta) + [20Dx\omega^2(\omega^2+\zeta^2) - 40Dx\omega^3\zeta + 12Dg\omega^2(\omega^2+\zeta^2) - 24Dg\omega^3\zeta]/(\omega^2-\zeta^2)^2$
0	2	1^{1+}	$2\omega + 4x + g - \zeta/2 + 4D\omega^2\zeta/(\omega^2-\zeta^2) + [4Dx\omega^2(\omega^2+\zeta^2) - 32Dx\omega^3\zeta - 4Dg\omega^2(\omega^2+\zeta^2)]/(\omega^2-\zeta^2)^2$
0	3	2^0	$3\omega + 9x - \zeta/2 + 2D\omega^2(3\zeta-\omega)/(\omega^2-\zeta^2) + [18Dx\omega^2(\omega^2+\zeta^2) - 76Dx\omega^3\zeta + 6Dg\omega^2(\omega^2+\zeta^2) - 4Dg\omega^3\zeta]/(\omega^2-\zeta^2)^2$
1	2	2^{2-}	$3\omega + 9x + 4g - \zeta/2 + 2D\omega^2(3\zeta+\omega)/(\omega^2-\zeta^2) - [6Dx\omega^2(\omega^2+\zeta^2) + 68Dx\omega^3\zeta + 18Dg\omega^2(\omega^2+\zeta^2) + 12Dg\omega^3\zeta]/(\omega^2-\zeta^2)^2$
2	1	2^{2+}	$3\omega + 9x + 4g - \zeta/2 - 6D\omega^2/(\omega+\zeta) + [42Dx\omega^2(\omega^2+\zeta^2) - 84Dx\omega^3\zeta + 30Dg\omega^2(\omega^2+\zeta^2) - 60Dg\omega^3\zeta]/(\omega^2-\zeta^2)^2$
0	4	3^{1-}	$4\omega + 16x + g - \zeta/2 + 8D\omega^2\zeta/(\omega^2-\zeta^2) + [8Dx\omega^2(\omega^2+\zeta^2) - 128Dx\omega^3\zeta - 8Dg\omega^2(\omega^2+\zeta^2)]/(\omega^2-\zeta^2)^2$
1	3	3^{1+}	$4\omega + 16x + g - \zeta/2 + 4D\omega^2(2\zeta-\omega)/(\omega^2-\zeta^2) + [40Dx\omega^2(\omega^2+\zeta^2) - 136Dx\omega^3\zeta + 24Dg\omega^2(\omega^2+\zeta^2) - 24Dg\omega^3\zeta]/(\omega^2-\zeta^2)^2$
2	2	3^{3-}	$4\omega + 16x + 9g - \zeta/2 + 4D\omega^2(2\zeta+\omega)/(\omega^2-\zeta^2) - [24Dx\omega^2(\omega^2+\zeta^2) + 120Dx\omega^3\zeta + 40Dg\omega^2(\omega^2+\zeta^2) + 40Dg\omega^3\zeta]/(\omega^2-\zeta^2)^2$
3	1	3^{3+}	$4\omega + 16x + 9g - \zeta/2 - 8D\omega^2/(\omega+\zeta) + [72Dx\omega^2(\omega^2+\zeta^2) - 144Dx\omega^3\zeta + 56Dg\omega^2(\omega^2+\zeta^2) - 112Dg\omega^3\zeta]/(\omega^2-\zeta^2)^2$

[a] Expressions for the analogous levels of the upper spin–orbit state are obtained by reversing the sign of ζ everywhere it appears. These results are calculated using the results of second-order perturbation energy according to formulas (B10a) and (B10b). The $\pm$ signs associated with v^l simply designate whether the level is raised (+) or lowered (−) as the Jahn–Teller coupling D is increased from zero.

for $p = 1, 3, 5, \ldots$,

$$E_p = (m+p)\omega + (m+p)^2x + m^2g \mp \zeta/2 + D\omega^2(p-1)/[\omega + (2m+2p-1)x - (2m+1)g \mp \zeta] - D\omega^2(2m+p+1)/[\omega + (2m+2p+1)x + (2m+1)g \pm \zeta] \quad \text{(B9a)}$$

and for $p = 2, 4, 6, \ldots$,

$$E_p = (m+p)\omega + (m+p)^2x + (m+1)^2g \pm \zeta/2 + D\omega^2(2m+p)/[\omega + (2m+2p-1)x + (2m+1)g \pm \zeta] - (pD\omega^2)/[\omega + (2m+2p+1)x - (2m+1)g \mp \zeta]. \quad \text{(B9b)}$$

These expressions simplify further if $|x| \ll |(\omega \pm \zeta)|/(2m+2p)$ and $|g| \ll |(\omega \pm \zeta)|/(2m+1)$, giving for $p = 1, 3, 5, \ldots$,

$$E_p = (m+p)\omega + (m+p)^2x + m^2g \pm \zeta/2 - (2m+2)D\omega^3/(\omega^2-\zeta^2) \mp 2(m+p)D\omega^2\zeta/(\omega^2-\zeta^2) + (m+p)(4m+6)Dx(\omega^4+\omega^2\zeta^2)/(\omega^2-\zeta^2)^2 \pm 4(2m^2+4mp+2p^2+m+1)Dx\omega^3\zeta/(\omega^2-\zeta^2)^2 + (m+p)(4m+2)Dg(\omega^4+\omega^2\zeta^2)/(\omega^2-\zeta^2)^2 \pm 4(2m^2+3m+1)Dg\omega^3\zeta/(\omega^2-\zeta^2)^2 \quad \text{(B10a)}$$

and for $p = 2, 4, 6, \ldots$,

$$E_p = (m+p)\omega + (m+p)^2x + (m+1)^2g \pm \zeta/2 + 2mD\omega^3/(\omega^2-\zeta^2) \mp 2(m+p)D\omega^2\zeta/(\omega^2-\zeta^2) + (m+p)(2-4m)Dx(\omega^4+\omega^2\zeta^2)/(\omega^2-\zeta^2)^2 \pm 4(2p^2+2m^2+4mp-m)Dx\omega^3\zeta/(\omega^2-\zeta^2)^2 - (m+p)(4m+2)Dg(\omega^4+\omega^2\zeta^2)/(\omega^2-\zeta^2)^2 \pm 4(2m^2+m)Dg\omega^3\zeta/(\omega^2-\zeta^2)^2. \quad \text{(B10b)}$$

In Eq. (B10a), the $\pm$ signs have been reversed to establish the convention that the upper/lower signs refer to the upper/lower spin–orbit level (assuming $\zeta > 0$). Identifying the coefficient of g as l^2 and the coefficient of ω as $v + 1$, the lowest vibronic levels v^l are obtained as listed in Table IV.

[1] K. Balasubramanian, J. Mol. Struct. (Theochem) **202**, 291 (1989).
[2] H. Åkeby, I. Panas, L. G. M. Pettersson, P. Siegbahn, and U. Wahlgren, J. Phys. Chem. **94**, 5471 (1990).
[3] E. Miyoshi, H. Tatewaki, and T. Nakamura, J. Chem. Phys. **76**, 5073 (1982).
[4] E. Miyoshi, H. Tatewaki, and T. Nakamura, Int. J. Quantum Chem. **23**, 1201 (1983).
[5] E. Miyoshi, H. Tatewaki, and T. Nakamura, J. Chem. Phys. **78**, 815 (1983).
[6] J. Flad, G. Igel-mann, H. Preuss, and H. Stoll, Surf. Sci. **156**, 379 (1985).
[7] C. Bachmann, J. Demuynck, and A. Veillard, Faraday Discuss. Chem. Soc. **14**, 170 (1980).
[8] J. Demuynck, M.-M. Rohmer, A. Strich, and A. Veillard, J. Chem. Phys. **75**, 3443 (1981).
[9] D. Post and E. Baerends, Chem. Phys. Lett. **86**, 176 (1982).
[10] A. B. Anderson, J. Chem. Phys. **68**, 1744 (1978).
[11] S. C. Richtsmeier, R. A. Eades, D. A. Dixon, and J. L. Gole, Am. Chem. Soc. Symp. Ser. **179**, 177 (1982).
[12] S. C. Richtsmeier, J. L. Gole, and D. A. Dixon, Proc. Natl. Acad. Sci. U.S.A. **77**, 5611 (1980).
[13] K. Balasubramanian and M. Z. Liao, J. Chem. Phys. **86**, 5587 (1987).
[14] K. Balasubramanian and M. Z. Liao, Chem. Phys. **127**, 313 (1988).
[15] C. W. Bauschlicher, Jr., Chem. Phys. Lett. **156**, 91 (1989).
[16] S. P. Walch and B. C. Laskowski, J. Chem. Phys. **84**, 2734 (1986).
[17] S. P. Walch, C. W. Bauschlicher, Jr., and S. R. Langhoff, J. Chem. Phys. **85**, 5900 (1986).
[18] C. W. Bauschlicher, Jr., S. R. Langhoff, and H. Partridge, J. Chem. Phys. **91**, 2412 (1989).
[19] H. Partridge, C. W. Bauschlicher, Jr., and S. R. Langhoff, Chem. Phys. Lett. **175**, 531 (1990).
[20] J. Ho, K. M. Ervin, and W. C. Lineberger, J. Chem. Phys. **93**, 6987 (1990).
[21] L.-S. Zheng, C. M. Karner, P. J. Brucat, S. H. Yang, C. L. Pettiette, M. J. Craycraft, and R. E. Smalley, J. Chem. Phys. **85**, 1681 (1986).
[22] C. L. Pettiette, S. H. Yang, M. J. Craycraft, J. Conceicao, R. T. Laaksonen, O. Cheshnovsky, and R. E. Smalley, J. Chem. Phys. **88**, 5377 (1988).
[23] O. Cheshnovsky, K. J. Taylor, J. Conceicao, and R. E. Smalley, Phys.

Rev. Lett. **64**, 1785 (1990).
[24] D. Schmeißer, K. Jacobi, and D. M. Kolb, J. Chem. Phys. **75**, 5300 (1981).
[25] M. Moskovits and J. E. Hulse, J. Chem. Phys. **67**, 4271 (1977).
[26] P. A. Montano, J. Zhao, M. Ramanathan, G. K. Shenoy, W. Schulze, and J. Urban, Chem. Phys. Lett. **164**, 126 (1989).
[27] A. Balerna, E. Bernieri, P. Picozzi, A. Reale, S. Santucci, E. Burattini, and S. Mobilio, Surf. Sci. **156**, 206 (1985).
[28] G. A. Ozin and H. Huber, Inorg. Chem. **17**, 155 (1978).
[29] W. E. Klotzbücher and G. A. Ozin, Inorg. Chem. **19**, 3767 (1980).
[30] T. Welker and T. P. Martin, J. Chem. Phys. **70**, 5683 (1979).
[31] M. F. Jarrold and K. M. Creegan, Chem. Phys. Lett. **166**, 116 (1990).
[32] D. R. Preuss, S. A. Pace, and J. L. Gole, J. Chem. Phys. **71**, 3553 (1979).
[33] M. D. Morse, J. B. Hopkins, P. R. R. Langridge-Smith, and R. E. Smalley, J. Chem. Phys. **79**, 5316 (1983).
[34] E. A. Rohlfing and J. J. Valentini, Chem. Phys. Lett. **126**, 113 (1986).
[35] M. D. Morse, Chem. Phys. Lett. **133**, 8 (1987).
[36] M. D. Morse, Chem. Rev. **86**, 1049 (1986).
[37] A. O'Keefe, J. J. Scherer, A. L. Cooksy, R. Sheeks, J. Heath, and R. J. Saykally, Chem. Phys. Lett. **172**, 214 (1990).
[38] P. Y. Cheng and M. A. Duncan, Chem. Phys. Lett. **152**, 341 (1988).
[39] J. A. Howard, R. Sutcliffe, and B. Mile, J. Chem. Soc. Chem. Commun. **1983**, 1449.
[40] K. Hilpert and K. A. Gingerich, Ber. Bunsenges. Phys. Chem. **84**, 739 (1980).
[41] W. Harbich, S. Fedrigo, J. Buttet, and D. M. Lindsay, Z. Phys. D **19**, 157 (1991).
[42] W. Harbich, S. Fedrigo, J. Buttet, and D. M. Lindsay, Mater. Res. Soc. Symp. Ser. **206**, 369 (1991).
[43] G. A. Bishea, C. A. Arrington, J. M. Behm, and M. D. Morse, J. Chem. Phys. **95**, 8765 (1991).
[44] G. A. Bishea and M. D. Morse, J. Chem. Phys. **95**, 5646 (1991).
[45] L. L. Ames and R. F. Barrow, Trans. Faraday Soc. **63**, 39 (1967).
[46] B. Simard, P. A. Hackett, A. M. James, and P. R. R. Langridge-Smith, Chem. Phys. Lett. (to be published).
[47] Z.-W. Fu, G. W. Lemire, Y. Hamrick, S. Taylor, J.-C. Shui, and M. D. Morse, J. Chem. Phys. **88**, 3524 (1989).
[48] S. C. O'Brien, Y. Liu, Q. Zhang, J. R. Heath, F. K. Tittel, R. F. Curl, and R. E. Smalley, J. Chem. Phys. **84**, 4074 (1986).
[49] W. C. Wiley and I. H. McLaren, Rev. Sci. Instrum. **26**, 1150 (1955).
[50] Philip R. Bevington, *Data Reduction and Error Analysis for the Physical Sciences* (McGraw-Hill, New York, 1969), *CURFIT* program, pp. 235–245.
[51] A. D. Sappey, J. E. Harrington, and J. C. Weisshaar, J. Chem. Phys. **91**, 3854 (1989).
[52] A. M. James, G. W. Lemire, and P. R. R. Langridge-Smith (unpublished results).
[53] G. A. Bishea, J. C. Pinegar, and M. D. Morse, J. Chem. Phys. **95**, 5630 (1991).
[54] G. Herzberg, *Molecular Spectra and Molecular Structure III. Electronic Spectra and Electronic Structure of Polyatomic Molecules* (Van Nostrand–Reinhold, New York, 1966), pp. 26–65.
[55] G. Duxbury, Specialist Periodical Report, Mol. Spectrosc. 3, Chemical Society, Burlington House, London, 1975, pp. 497–573.
[56] Ch. Jungen and A. J. Merer, in *Molecular Spectroscopy: Modern Research*, edited by K. N. Rao (Academic, New York, 1976), Vol. 2, pp. 127–164.
[57] J. M. Brown and F. Jørgenson, Adv. Chem. Phys. **52**, 117 (1983).
[58] R. Englman, *The Jahn–Teller Effect in Molecules and Crystals* (Wiley-Interscience, London, 1972).
[59] I. B. Bersuker, *The Jahn–Teller Effect: A Bibliographic Review* (IFI Plenum, New York, 1984).
[60] I. B. Bersuker, *The Jahn–Teller Effect and Vibronic Interactions in Modern Chemistry* (Plenum, New York, 1984).
[61] W. Moffitt and W. Thorson, Phys. Rev. **108**, 1251 (1957).
[62] H. C. Longuet-Higgins, U. Öpik, M. H. L. Pryce, and R. A. Sack, Proc. R. Soc. London Ser. A **244**, 1 (1958).
[63] M. S. Child and H. C. Longuet-Higgins, Philos. Trans. R. Soc. **254**, 259 (1962).
[64] M. S. Child, J. Mol. Spectrosc. **10**, 357 (1963).
[65] F. T. Chau and L. Karlsson, Phys. Scr. **16**, 248 (1977).
[66] W. H. Gerber and E. Schumacher, J. Chem. Phys. **69**, 1692 (1978).
[67] F. T. Chau and L. Karlsson, Phys. Scr. **16**, 258 (1977).
[68] F. S. Ham, Phys. Rev. A **138**, 1727 (1965).
[69] H. Lefebvre-Brion and R. W. Field, *Perturbations in the Spectra of Diatomic Molecules* (Academic, Orlando, 1986), p. 215.
[70] L. Pauling and E. B. Wilson, Jr., *Introduction to Quantum Mechanics* (Dover, New York, 1963), pp. 105–11.
[71] C. H. Townes and A. L. Schawlow, *Microwave Spectroscopy* (Dover, New York, 1975), p. 32.